Theor Chem Acc (2007) 117:765–779
DOI 10.1007/s00214-006-0199-9

REGULAR ARTICLE

The role of quantum chemistry in the elucidation of the elementary mechanisms of catalytic processes: from atoms, to surfaces, to enzymes

Monica Leopoldini · Tiziana Marino · Maria del Carmen Michelini · Ivan Rivalta · Nino Russo · Emilia Sicilia · Marirosa Toscano

Received: 13 October 2006 / Accepted: 13 October 2006 / Published online: 6 February 2007

Abstract The recent activity of the laboratory of quantum and computational chemistry of the University of Calabria in the field of catalysis is shortly reviewed. Theoretical determinations of the potential energy profiles for the cyclotrimerization of acetylene catalyzed by bare and supported niobium atom and the reduction mechanism of nitrate to nitrite by nitrate reductase enzyme are presented as examples of studies in which a certain number of investigation methods mostly used in this field, are applied.

Keywords Catalysis · DFT · PES · Metalloenzymes · Clusters

1 Introduction

One of the most interesting research field of chemistry in the 1900s is that of catalysis. Really, the history of catalysis is much older since the nature invented it in the early stage of the vegetal and animal kingdoms. In fact, in the living organisms an enormous number of known and unknown reactions, necessary to their functionality, are catalyzed by special catalysts—the enzymes. The number of Nobel prizes assigned in this period to the scientists who contributed in this field demonstrates its importance. The continuous attention devoted to the catalytic processes is dictated essentially by their industrial applications that permeate every day many human activities. The interest of scientists is also, or better mainly, due to the desire to understand and explain the elementary mechanisms which catalytic phenomena are based on. Nowadays, an incredible number of industrial-manufactured articles (e.g. gasoline, plastic materials, drugs, etc.) are produced by using catalyzed reactions.

Traditionally, catalysis is classified as homogeneous and heterogeneous depending on the fact that catalyst has or not the same phase of reactants. The extremely important group of enzymes cannot be accommodated within this classification. In fact, they are neither homogeneous nor heterogeneous catalysts. We must therefore regard enzymatic catalysis as something quite different from the other two forms of catalysis.

In the major part of the catalysts operating in homogeneous and heterogeneous phases as well as in the enzymes, metal species are frequently involved (often a transition metal). The main difference of these catalysts lies in the different coordination around the metal center, so that, studies on the elementary mechanism of reaction catalyzed by metal-containing systems can contribute not only to elucidate the specific reaction but also to build up an "unified theory" of catalysis.

Quantum chemical methods can play an important role in understanding catalysis because they provide some advantages such as the localization and characterization of reaction intermediates and transition states and the individuation of different possible reaction pathways.

Among them, the methods based on the density functional theory (DFT) appear to be highly accurate and in competition with the most reliable ab initio-CI methods.

M. Leopoldini · T. Marino · M. del Carmen Michelini · I. Rivalta · N. Russo (✉) · E. Sicilia · M. Toscano
Dipartimento di Chimica and Centro di Calcolo ad Alte Prestazioni per Elaborazioni Parallele e Distribuite-Centro d'Eccellenza MIUR, Universita' della Calabria, Arcavacata di Rende (CS) 87030, Italy
e-mail: mrusso@unical.it

In fact, the DFT allows the treatment of large systems, because of the reduced computational efforts.

Gas-phase studies on "isolated" reactants provide an ideal way to investigate in detail the energetics and kinetics of any bond-making and bond-breaking process at a strictly molecular level. In the last decades many experimental and theoretical works have been exploited to provide useful insight into the elementary steps of various catalytic reactions and to characterize reactive intermediates that have been previously out of condensed-phase techniques (see example [1–7]). Clearly, as a result of the absence of counterions, solvation, and any environmental influence, these coordinatively unsaturated ("naked") species will, in general, be much more reactive than their condensed-phase analogs [8–11]. Thus, gas-phase studies will, in principle, never account for the precise mechanisms, energetics, and kinetics operating in applied catalysis. However, such experimental studies, are not at all without meaning, as they provide a conceptual framework and an efficient mean to obtain direct insight into reactivity patterns, the role of differential ligation, the importance of aspects of electronic structure, and the nature of crucial intermediates. Furthermore, as these gas-phase studies can be performed under well-defined conditions, they play a key role in the evolution of approaches aimed at a more comprehensive understanding of elementary steps, knowledge of which is mandatory for the design of tailor-made catalysts [1–7,12–31].

To better reproduce the "real-life" catalysts three different techniques are currently used to model the structure at the active site. These are known as cluster [32–34], embedded cluster [35–39], and periodic methods [40–44]. Each method has its own set of advantages and disadvantages. In the cluster approach, a discrete number of atoms is used to represent the active site region. The basic idea is that chemisorption and reactivity are local phenomena, primarily affected only by the nearby surface structure. The embedded cluster model is an extension of the cluster approach whereby the problems associated with the abrupt cluster termination are treated by embedding the cluster into a lower level quantum mechanical or molecular mechanical model. In the embedded cluster approach, a rigorous quantum mechanical (QM) method is used to model the local region about the active site. This primary cluster is then embedded into a much larger system in order to simulate the external electronic environment. The outer model employs a much simpler quantum mechanical treatment or an empirical force field to simulate the external environment. This minimizes cluster-size artifacts. The outer model can subsequently be embedded in yet a third model which is made of point charges to treat the Madelung potential. The last approach is the periodic slab method. In this method one defines a unit cell which comprises a large enough surface ensemble. Periodic boundary conditions are then used to expand the cell in x, y, and/or z directions, thus providing the electronic structure for linear, slab (surface), and bulk materials, respectively.

As far as the enzymatic catalysis is concerned, the systems studied experimentally in this field are usually excessively large for a quantum chemical treatment, thus, notwithstanding the current computer power that allows the investigation of systems of noticeable dimensions, some stratagem is mandatory.

For instance, the enzyme active sites can be investigated using model systems including at least the first coordination shell of metal centers. Nevertheless, sometimes this choice is insufficient to describe correctly the reaction, thus some second shell residues, which the experiment indicates to be active in the development of the enzymatic process, must be included explicitly. Furthermore, if the active site is particularly large, some of the ligands that do not directly participate in the catalytic process, can be replaced by simpler ligands.

The remaining part of the enzyme can be considered as a homogeneous polarizable medium, and can be described by one of the available continuum solvation methods using an opportune dielectric constant that simulates a protein like environmental [45,46]. The standard value is epsilon = 4. The PCM [47–49] model calculates the free energy in solution as the sum of three terms that represent the electrostatic and the dispersion–repulsion contributions to the free energy, and the cavitation energy. All three terms are calculated using a cavity determined from a surface of constant charge density around the solute molecule. The reaction field is represented through point charges located on the surface of the molecular cavity.

Alternatively, we can resort to the QM/MM hybrid methods [50]. The general idea on which these methods are based is that a chemical system made up of hundreds or thousands of atoms can be partitioned into a region electronically important that requires a QM treatment and into a second region that acts in a perturbative way on the first one and allows a classic description molecular mechanics (MM).

Among the QM/MM, the ONIOM methods are extensively used [51–57] to compute potential-energy profiles for biologically large systems and provide reliable information about the influence of the protein environment on active site structures and reaction energetics.

In the ONIOM procedure, the system is described through a model divided into two parts, an inner and an outer layer. The inner layer consists of a metal center

and its first coordination sphere. The outer layer is made up of some amino acids, fixed at their crystallographic positions to prevent optimization from giving an unrealistic expansion of the protein [58]. Hydrogen atoms can be used to saturate fragments from the Protein Data Bank (PDB) structure, avoiding chemical artifacts.

For the ONIOM study, quantum mechanical and molecular mechanics UFF force fields [59] can be used to perform high-level and low-level inner-layer calculations, respectively.

Recently, a new approach, the so-called Orbital-Free Embedding method [60] was proposed to study also the enzymatic reaction. This method, contrary to the hybrid QM/MM ones, does not depend on the parameters and calibration used [61]. The orbital-free embedding scheme allows the description of different regions of a system of interest on different levels of theory. Kohn–Sham-like equations are solved to obtain the electron density of a fragment (i.e. active site of enzyme), which is embedded in a larger frozen system (protein environment).

The fact that the studied subsystem is embedded in a microscopic environment is represented in this formalism by means of a special term in the effective potential—effective embedding potential. This embedding potential is system-independent because it uses the universal functionals of electron density. It is expressed as a function of two variables ρ_A and ρ_B which are the electron densities of the embedded system and its microscopic environment, respectively. It is, therefore, orbital-free. The explicit analytic form of the orbital-free embedding effective potential is not known, but it can be expressed using approximations to the non-additive kinetic energy functional (the difference between the kinetic energy $T_s[\rho]$ of the total electron densities and that of the separated electron densities of the two subsystems) and the exchange-correlation functional defined in the Kohn–Sham formalism [60,61].

2 Computational details

GAUSSIAN 03 code was used for all computations reported here [62]. An efficient computer implementations of the orbital-free embedding deMon2K-KSCED [63] based on the code deMon2K [64] solving Kohn–Sham equations was only employed in the study of nitrate reductase enzyme.

For the investigation of the acetylene cyclotrimerization reaction mediated by Nb naked atom, the Becke's three-parameter hybrid functional [65] combined with the Lee, Yang, and Parr (LYP) [66] correlation functional, was employed. The LANL2DZ effective core potential [67–69] and the standard 6−311+G** basis set [70,71] were used for the metal center and the rest of the atoms, respectively.

The study of acetylene cyclotrimerization on Nb_1/MgO(100) was performed using the 6-31G basis for Mg atoms. Nb atom was described by the LanL2DZ ECP [67–69] pseudopotential, while C, O, and H were treated with a 6-31G* basis set. Frequency calculations of the saddle-point structures show the existence of only one negative frequency value associated to the vibrational mode of the reaction coordination chosen for the reaction path. The calculations have been performed at the spin-polarized DFT level with the B3LYP functional.

For nitrate reductase, optimization, and vibrational analysis were carried out using B3LYP/6-31+G* [65,66,70,71] density functional protocol. PW91PW91/6-31+G* [72–76] method was then used to perform single point computations on B3LYP/6-31+G* [65,66,70,71] optimized geometries. LANL2DZ [67–69] pseudopotential for the metal ion was chosen in both set of calculations. Although the involvement of two spin-states in oxo-transfer reaction catalyzed by molybdoenzyme-analogous systems was never claimed out previously, we examined singlet and triplet energy profiles using restricted closed-shell and unrestricted open-shell approaches, respectively. No spin contamination was found for triplet species ($\langle S^2 \rangle$ value was about 2 in all cases).

The PW91PW91 exchange-correlation functional was used in both Kohn–Sham and KSCED calculations in connection with DZVP basis set [77] and the automatically generated auxiliary A2* functions [78].

3 Results and discussion

3.1 Acetylene cyclotrimerization mediated by the bare Nb atom

In the framework of a more extended project aimed to unravel the elementary mechanisms of catalytic processes for the activation of prototypical bonds mediated by transition metal-containing systems, we have undertaken a systematic theoretical study of the cyclotrimerization of acetylene mediated by bare second-row transition metal atoms.

Cycloaddition of unsaturated hydrocarbons is a useful kind of reaction for the synthesis of organic ring systems. Although these reactions are generally quite exothermic, they are usually hampered by high kinetic barriers as long as non-activated hydrocarbons are involved. Thermal cyclotrimerization of acetylene to form benzene is particularly interesting from this point of view

since, even if this transformation is extremely exothermic, of about 142 kcal/mol [79], it takes place only at temperatures higher than 400 °C. The results of the theoretical calculations performed on cyclotrimerization of acetylene have evidenced that high temperatures are required to overcome a prohibitive activation barrier calculated to lie in the 60–80 kcal/mol regime [80,81]. Thus, the synthetic advantages this reaction possess cannot be exploited unless catalysts are used. Since the first announcement of acetylene cyclotrimerization on Pd at low temperatures [82–84] a lot of theoretical and experimental studies, covering many structural, mechanistic, and kinetic aspects, have appeared in literature dealing with acetylene cyclotrimerization to give benzene catalyzed by transition metals from bare and supported atoms to crystals [85–99]. However, they essentially concern the reactivity of late transition metals, particularly those from group 8, while the possibility to use early transition metals as catalysts to increase the rate of the studied process and to allow the use of milder reaction conditions has been less extensively explored [100].

Here are presented the results of the theoretical investigation of the acetylene cyclotrimerization reaction mediated by a naked atom form the left-hand side of 4d series that is Nb.

The study of the mechanism of benzene formation was carried out from the hypothesis that the reaction proceeds through the consecutive addition of acetylene molecules without C–C bond scission. The possible alternative steps that can occur after adsorption of a second acetylene molecule have been taken into account as reported in Scheme 1. Indeed, the two acetylene molecules can isomerize to form a complex containing a metallacycle (MC_4H_4) or a cyclobutadiene molecule bonded to the metal M–C_4H_4 or the M–$(C_2H_2)_2$ complex can prefer to adsorb a third one. As a consequence the three acetylene molecules can isomerize in a concerted way to lead directly to the benzene formation or from one of the MC_4H_4 or M–C_4H_4 complexes the corresponding (C_2H_2)–MC_4H_4 and (C_2H_2)–M–C_4H_4 ones are formed. Finally, once one or the other of these latter two complexes is formed the reaction can pass through a new metallacycle reaction intermediate MC_6H_6 before the benzene formation, M–C_6H_6.

The mechanistic details of the reaction under examination have been studied in accordance with the two-state reactivity (TSR) paradigm [101], whose central idea was introduced, at first, by Armentrout and coworkers [102,103]. Due to accessibility of the excited states of the considered atom, it cannot be excluded the possibility of spin crossing between surfaces of different multiplicity.

In our investigation for benzene formation from acetylene mediated by Nb, according to the sequence of steps proposed into the schematic representation of the mechanism (see Scheme 1), the formation of all the possible complexes has been taken into consideration.

The cyclotrimerization process takes place via the following steps: (a) coordination and activation of an acetylene molecule; (b) coordination and activation of a second acetylene molecule to form a M–$(C_2H_2)_2$ complex; (c) formation of a metallacycle, MC_4H_4, complex that implies overcoming a barrier for the first transition state of the reaction; (d) coordination and activation of a third acetylene molecule to form a (C_2H_2)–MC_4H_4 complex; (e)formation of a MC_6H_6 metallacycle intermediate that again implies overcoming an energy barrier for the second transition state along the reaction path; (f) formation of a final complex corresponding to benzene formation through a third transition state followed by benzene elimination.

The possibility that the reaction goes through the formation of a M–C_4H_4 complex was ruled out since this intermediate lies higher in energy with respect to the corresponding metallacycle complex. In the same way, any attempt to follow the pathway that from three acetylene molecules leads directly to benzene formation through a concerted mechanism, was unsuccessful.

The potential energy surfaces for the complete cyclotrimerization of acetylene to give benzene is reported in Fig. 1.

Relative energies are reported with respect to the reactants' limit represented by the isolated metal atom in its ground state and three acetylene molecules, and have been corrected for ZPE but not for BSSE to allow a fair comparison between minima and transition states.

In order to evidence the possibility of spin crossing between PESs of different multiplicity it was necessary to investigate three different spin states. Even if a correct energetic ordering of the ground and excited states is predicted, theoretical gaps are overestimated with respect to the experimental ones [104]. Indeed, the ground state of Nb atom, ^6D ($4d^45s$), lies 11.1 kcal/mol lower in energy than the ^4F ($4d^35s^2$) state and 36.7 kcal/mol lower than the ^2G ($4d^35s^2$) state, whereas the corresponding experimental gaps are 4.3 and 24.3 kcal/mol, respectively.

The first step of the reaction is the coordination and activation of one acetylene molecule that occurs through a Chatt–Dewar–Duncanson (CDD) mechanism [105, 106] in which acetylene donates parts of the π electrons to an empty σ-orbital of the metal. As a consequence, the π bond of acetylene is weakened and the π^*-orbital is lowered in energy so that electrons can be accepted

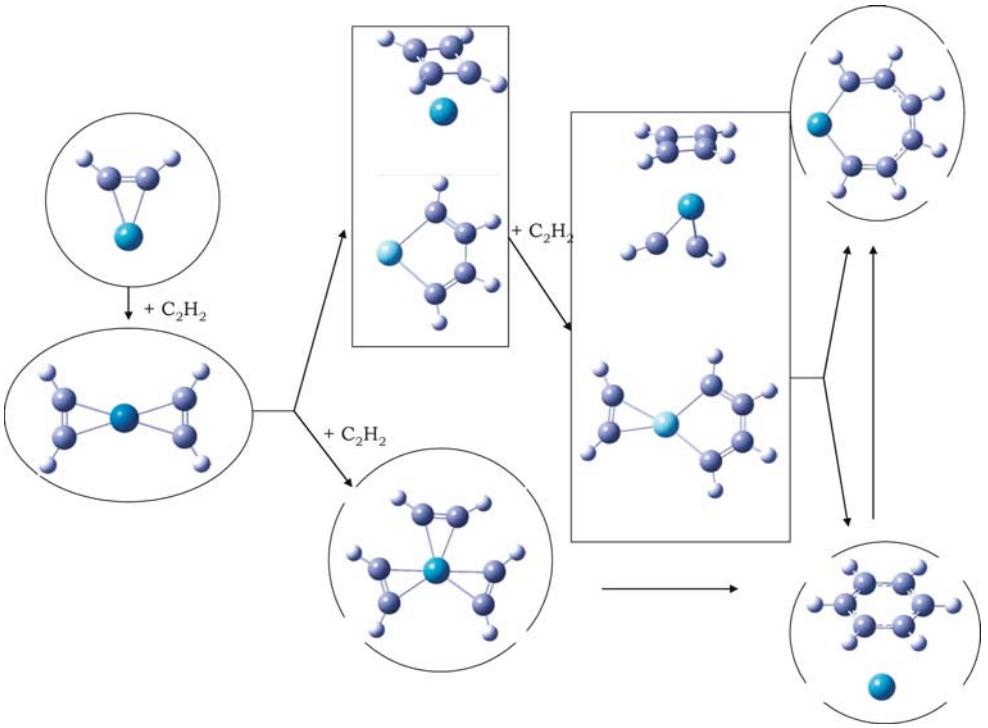

Scheme 1 Schematic representation of the mechanism studied for the benzene formation from acetylene and naked transition metal atom

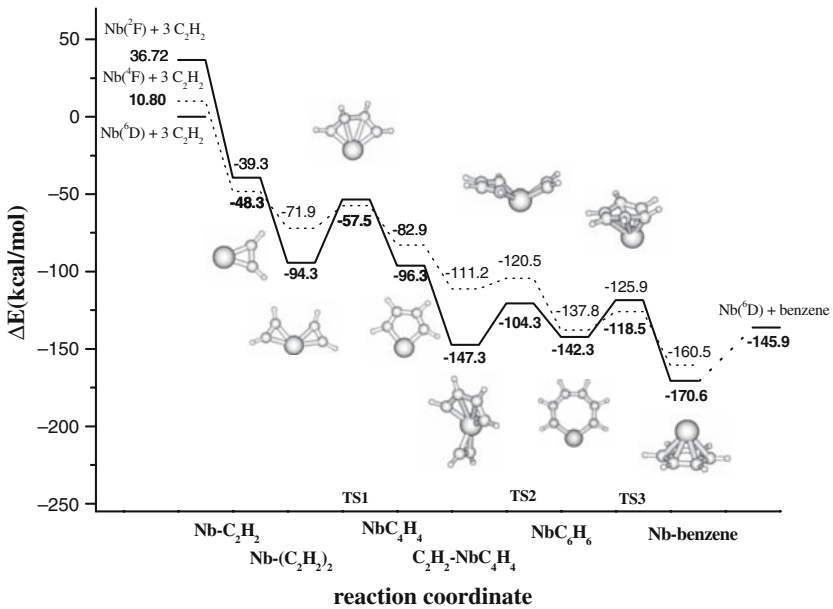

Fig. 1 Quartet and doublet potential energy surfaces for the reaction $Nb + 3C_2H_2$. Energies are in kcal/mol and relative to the sextet ground-state reactants

from a back-donating d-orbital of the metal atom. This description of the binding mechanism is very general and at least three different situations, that can be preferred by different transition metals, can be characterized. Indeed, the back-bonding donating d-orbital can be initially singly or doubly occupied or normal covalent bonds can be formed. Covalent bond formation, indeed, can be considered as an extreme of the donation bonding and leads to formation of a metallacyclopropane complex, so-called because the triple bond is broken and two covalent bonds are formed between the metal and the two carbon atoms in a three-member ring [107]. The latter description of the interaction describes exactly what occurs for Nb atom as it inserts into the in-plane π bond of acetylene forming a metallacyclic compound. The definitive breaking of the π bond of the first

acetylene molecule is monitored both by the elongation of the C–C bond and the distortion of the bond angle H–C–C with respect to the gas-phase values (calculated d(C–C) = 1.206 Å) as well as by the short C–M bond distances. Computed binding energy is 48.34 kcal/mol and accounts also for the necessity to promote the atom to the appropriate binding $4d^{n+1}5s$ state. Indeed, the ground state of the complex does not correspond to the ground state of the bare metal atom for and this means that a spin crossing occurs at the entrance channel (see Fig. 1).

Coordination of a second acetylene molecule occurs with an energy release comparable to that for the first one. Indeed, the binding energy, calculated as $E[M(C_2H_2)_2] - E[(M(C_2H_2)] - E(C_2H_2)$, is 50.97 kcal/mol. The extent of the coordination depends again on the donation and back donation mechanism and can be measured by the gas-phase geometry distortion of the acetylene molecule. The C–C bond lengths for the two activated acetylene molecules in the complexes Nb–$(C_2H_2)_2$ are the same and significantly longer than the free molecule and again a metallacycle bisacetylene complexes, slightly distorted from planarity, is formed. As the ground state of the complex obtained by the coordination of the second acetylene molecule is doublet a new spin crossing occurs along the path.

The processes of acetylene coordination considered so far are not activated, whereas the oxidative coupling of acetylene to form a MC_4H_4 complex implies to surmount the first energy barrier for the process. The process involves the formation of a new σ bond between two C atoms of adjacent acetylene molecules and eventually of new σ M–C bonds at the expenses of π interactions in the $(MC_2H_2)_2$ complexes. The overall energetic balance due to bonding changes occurring during this transformation acts in such a way that the formation of the MC_4H_4 metallacycle intermediate is exothermic with respect to separated reactants ($M + 2C_2H_2$), whereas the conversion of the bisacetylene complex to the MC_4H_4 species is thermoneutral. The formed complex is not planar, the C–C distances are almost equal amongst them, the new C–C bond is almost formed but the two corresponding Nb–C bonds are not completely broken yet.

Location of the transition states for the conversion process reveals an energy barrier of 36.82 kcal/mol that implies a transition state structure geometrically dissimilar to the reactants. The transition state structure localized along the PES lie below the separate reactants' dissociation limit and, since its ground-state multiplicity changes, a spin crossing occurs even if ground spin state of reactant $(MC_2H_2)_2$ and product MC_4H_4 is the same.

Coordination of a third acetylene molecule to the metallacyclopentadiene complex represents a key step in the process toward benzene formation since it involves the metal ability to activate another acetylene molecule. Previous calculations showed that an unsupported Pd atom is unable to add and activate three acetylene molecules [108] and the step appears to be critical also in the case of transition metal complexes [109]. The bare metal atoms considered here show different behaviors. The activation of the third acetylene molecule is monitored again by the distortion of the geometrical parameters of the bonded molecule with respect to the gas-phase values. A considerable back-bonding interaction results in the elongation of the C–C bond and a reduction of the acetylenic C–C–H angle and the energy of the additional interaction amounts to 51.01 kcal/mol.

After the activation of the third acetylene two mechanisms for benzene formation appear conceivable that is the direct intermolecular cycloaddition of the coordinated acetylene to the MC_4H_4 intermediate or the insertion of the alkyne in the metal–carbon σ bond of the metallacyclopentadiene to form a new metallacycle intermediate. Although previous theoretical works on the same subject unfavorably considered the second route toward benzene formation, [61,62] any attempt to obtain benzene directly from intermediate C_2H_2–MC_4H_4 were unsuccessful and a stable metallacycle, MC_6H_6, was localized along the path together with the transition state corresponding to the formation of a C–C bond between the C_2H_2 and the C_4H_4 units. The insertion process appears to be slightly endothermic 5.01 kcal/mol and the energy barrier relative to the formation of the transition state amounts to 28.79 kcal/mol. For all the localized transition states both the check of the vibrational mode associated to the imaginary frequency and the IRC calculation confirmed that the transition state structures correspond to the insertion of the acetylene into the C–M bond of the MC_4H_4 moiety.

As a last step, benzene formation occurs via reductive elimination of the C_6H_6 bidentate ligand from the metallacycloheptatriene, MC_6H_6, complex through the formation of the final intermediate, M–C_6H_6, appearing in the catalytic cycle. To this step is associated an energy gain of 28.29 kcal/mol. The energy barrier that is necessary to overcome to obtain the final adduct, M–C_6H_6, is 23.79 kcal/mol and new spin crossings occur before and after the transition state formation lowering the energy barrier for the process.

In its equilibrium geometry formed benzene lies flat in the Nb complex and the computed interaction energies is 24.65 kcal/mol. So the rate determining step for the overall process corresponds to the formation of the

metallacyclopentadiene from the bisacetylene complex. All the minima are stable and the transition states in their ground states lie below the reactants dissociation limit. The combined thermodynamic and kinetic analysis of the process indicates that niobium can be considered a good candidate for the cyclization of acetylene to give benzene.

3.2 Acetylene cyclotrimerization on Nb_1/MgO(100)

The considered reaction of cyclization of acetylene to give benzene has been widely studied on single-crystal surfaces from UHV conditions (10^{-12}–10^{-8} atm) to atmospheric pressure (10^{-1}–1 atm) [82–86]. A Pd(111) surface is the most reactive one [84,87], and the experimental findings have added important information as, at high coverages, reactively formed benzene molecules are forced to adopt a tilted configuration, and therefore they interact weakly with the surface and desorb at low temperature [82,83]. As the surface becomes depleted of adsorbed species, the remaining reactively formed benzene molecules adopt a flat-lying, more strongly adsorbed configuration, eventually desorbing at ∼500 K [82,83].

Surface science studies have shown that the existence of an ensemble of three 3-fold sites on the Pd(111) surface is necessary for the reaction to occur [84,110] and that this can explain the surface sensitivity of the reaction. Very similar reaction patterns have also been observed on Al_2O_3-supported Pd particles of a few nanometer size as they exhibit (111) and (100) microfacets on their surface [85,111]. In view of the surface sensitivity of the reaction, it was considered rather surprising that in the experiments on size-selected Pd clusters on MgO thin films even a single Pd atom was able to induce the acetylene cyclization. A series of theoretical calculation has clearly shown that this is connected to the fact that the metal atom interacts with point defects at the surface of MgO with consequent increase of the charge density around the Pd atom which becomes an active single-atom catalyst [112].

Here, we present some of the results obtained carrying out a detailed DF theoretical study of the cyclization reaction mediated by the Nb atom on cluster model of the MgO support, looking at various types of morphological defects as well as at vacancy sites, and performing an accurate analysis of the electronic effects involved in the metal-support interaction. Even the role played by diffusion in influencing reactivity of the Nb-supported atom has been accounted for.

To establish the role of the regular and low-coordinated surface anions of MgO in modifying the properties of a supported Nb atom, we have considered three simple models. They represent five-, four-, and three-coordinated O anions at terrace, edge, and corner sites, respectively. Neutral (two electrons trapped into the vacancy), F_s, and positively charged (one electron trapped into the vacancy), F_s^+, oxygen vacancies have been modeled by removing the oxygen atom from the center of the corresponding clusters for terrace, edge, and corner sites.

An embedded cluster approach [113] was used to model the reaction occurring on Nb atoms adsorbed on different sites of the MgO surface and the cluster O_9Mg_5 was used to represent the terrace site. The corresponding terrace oxygen vacancy center (hereafter named F_{5c}) was obtained by removing the central oxygen atom of the cluster.

Due to the highly ionic nature of MgO, the truncation of the lattice in cluster calculations implies the use of an external field to represent the long-range Coulomb potential. The considered model cluster has been embedded in arrays of point charges (PC) (±2 e) in order to reproduce the correct Madelung potential at the adsorption site under study [114]. The occurrence of an artificial polarization of the oxide anions at the cluster border has been avoided by placing an effective core potential (ECP) on the positive charges around the quantum mechanical cluster. The whole system, cluster + ECPs + PCs is electrically neutral. The positions of the adsorbed molecules, of Nb atom and of their first neighbors on the MgO surface have been fully optimized with no symmetry constraints. The transition state (TS) search has been performed using the Berny algorithm and the nature of the TS has been verified by performing a frequency analysis. All the Nb surface complexes have sextet ground-state.

In Fig. 2 is reported the calculated PES for the cyclotrimerization reaction mediated by the Nb atom supported at a terrace oxygen vacancy center, F_{5c}, as they (as shown also by previous works [115]) are likely trapping sites for the metal atoms. In the inset is reported the structure of the MgO cluster embedded in ECPs and a large array of point charges.

As can be realized from Fig. 2 the steps of the reaction mediated by the Nb atom supported on MgO are the same for the reaction of the bare atom, i.e. coordination and activation of a single acetylene molecule, coordination of a second acetylene molecule and formation of an activated complex to give the C_4H_4 intermediate, coordination of a third acetylene molecule, formation of a new cyclic intermediate through a second activated complex, formation of adsorbed benzene and its subsequent desorption.

The Nb surface complex binds C_2H_2 by 29 kcal/mol. Upon adsorption, the C_2H_2 molecule becomes consid-

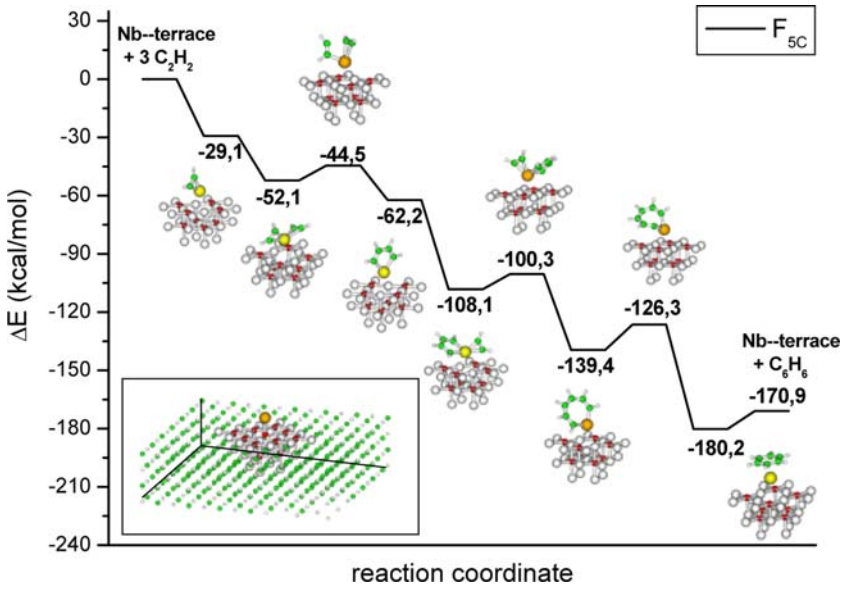

Fig. 2 Reaction path for acetylene cyclization on Nb supported on a charged oxygen vacancy at terrace (F_{5c}) site of the MgO surface. Energies are in kcal/mol. In the inset is reported the structure of the MgO cluster embedded in ECPs and a large array of point charges

erably activated as monitored by the distorted H–C–C angle, and by the elongation of the C–C distance with respect to the gas-phase value. Nb/F_{5c} binds a second C_2H_2 molecule by 23 kcal/mol with an energy release comparable to that for the first one. The oxidative coupling of acetylene to form C_4H_4 implies to overcome the energy barrier for the corresponding transition state. The process is exothermic by 10 kcal/mol, whereas the barrier height is 7.6 kcal/mol.

A third acetylene is added to the $Nb(C_4H_4)$ complex on an F center with a gain of 45.9 kcal/mol and the formed C_2H_2–NbC_4H_4 complex rearranges surmounting an energy barrier of 7.8 kcal/mol to yield the metalloeptacycle that is stabilized with respect to reactants asymptote by 139.4 kcal/mol. Benzene is formed with a large gain of 40.8 kcal/mol and by surpassing the highest energy barrier, that amounts to 13 kcal/mol, met along the energy profile for the conversion of acetylene to benzene promoted by an Nb atom supported on an MgO(001) terrace F site. Once formed benzene readily desorbs as is only weakly bonded to the supported Nb atom. The corresponding binding energy is indeed 9.3 kcal/mol.

To summarize, the overall $Nb + 3C_2H_2 \rightarrow Nb(C_6H_6)$ process on a terrace oxygen vacancy of the MgO support is thermodynamically much favored and includes three individual steps which imply overcoming energy barriers that are low and lie below the limit represented by ground-state reactants. The rate determining step appears to be formation of the adsorbed benzene from the seven members NbC_6H_6 cycle, while benzene is only weakly bound and readily desorbs.

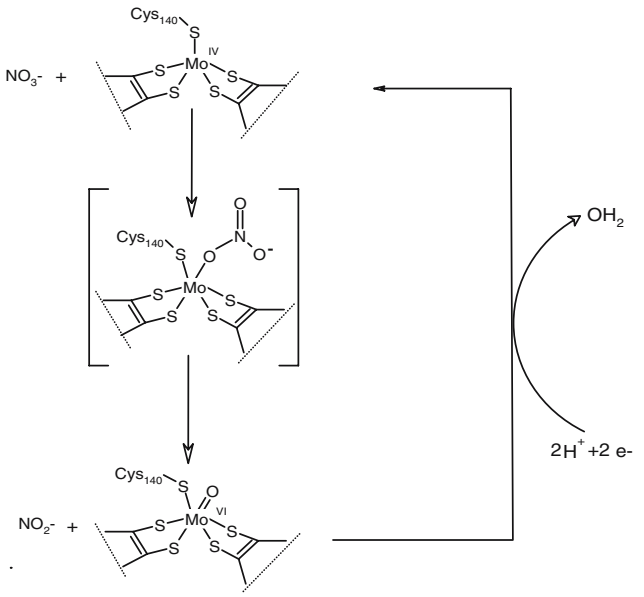

Scheme 2 Nitrate reductase catalytic cycle

3.3 Nitrate reductase molybdoenzyme

Nitrate reductase catalyzes the reduction of nitrate to nitrite assuming an important role in nitrogen assimilation [116].

The enzyme molecule consists of four domains involved in cofactor binding. One of these domains is responsible for the binding with an Fe_4S_4 cluster that serves as an electrons pump [117]. The two bismolybdopterin guanine dinucleotide cofactors present in the molecule are stabilized by a hydrogen bond's network

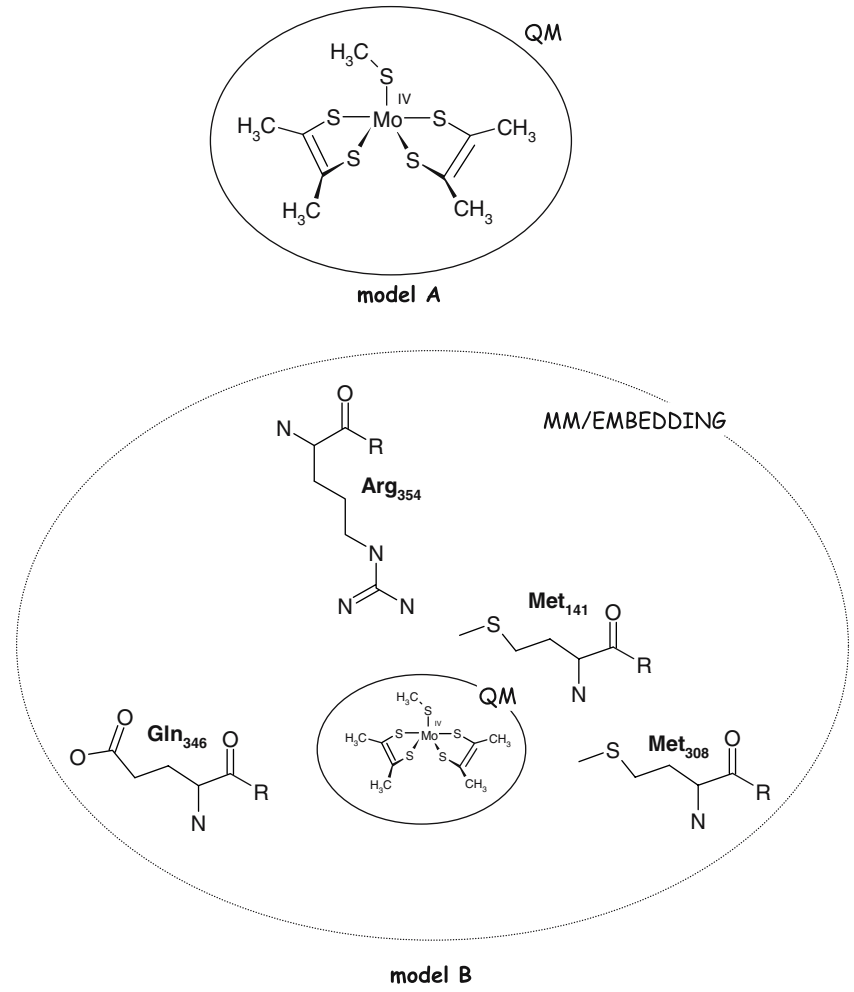

Fig. 3 Employed model systems

with amino acidic residues [117]. The Mo^{VI} metal center surrounding involves four sulphur atoms of two dithiolene groups, the sulphur atom of side chain of Cys140 residue and a hydroxo/water molecule that completes the coordination. Ligands are arranged in a distorted trigonal prismatic geometry.

Several charged residues, such as Arg354, Asp155, Glu156, Asp355, Ala142, Val145, Val149, Leu359, and Leu362 are present in the protein environment of active site. Arg354 was recognized as the site for the anchor of the negative charged nitrate. Furthermore, conserved residues among all nitrate reductases are Gln346, Met308, and Met141 [117].

Because of the lack of crystallographic data on the reduced Mo^{IV} nitrate reductase form, a catalytic mechanism based on the oxidized form behavior was suggested [117].

The nitrate reductase catalytic cycle is described in Scheme 2.

The five coordinated $Mo^{IV}(Mo^{IV}S^{Cys}(SR)_4)$ coordinates a nitrate ion. The bond of NO_3^- with the metallic center leads to a weakening of N–O bond. The Mo^{IV} is oxidized to Mo^{VI} and NO_2^- is released. Mo^{IV} is restored in another step, by two protons coming from water molecules present in the active site and two electrons coming from the Fe_4S_4 cluster.

In this work, two models were used for enzyme active site simulation. The first one (model A of Fig. 3) was the bisdimethyl dithiolene structure, previously proposed elsewhere [118]. An SCH_3 group was chosen to mimic Cys140 residue. The second model (model B of Fig. 3) was obtained adding to the model A four amino acid residues usually conserved within the family of nitrate reductases, namely Arg354, Gln346, Met308, and Met141, according to their crystallographic positions [117].

The B3LYP-optimized geometry for molybdenum (IV) model system A in its singlet electronic state was found to be square-pyramidal with Mo–S dithiolene average distances of 2.365 Å, and with a Mo–S^{Cys} bond length of 2.347 Å in agreement with experimental ones of Holm and coworkers for phenoxy complexes [119].

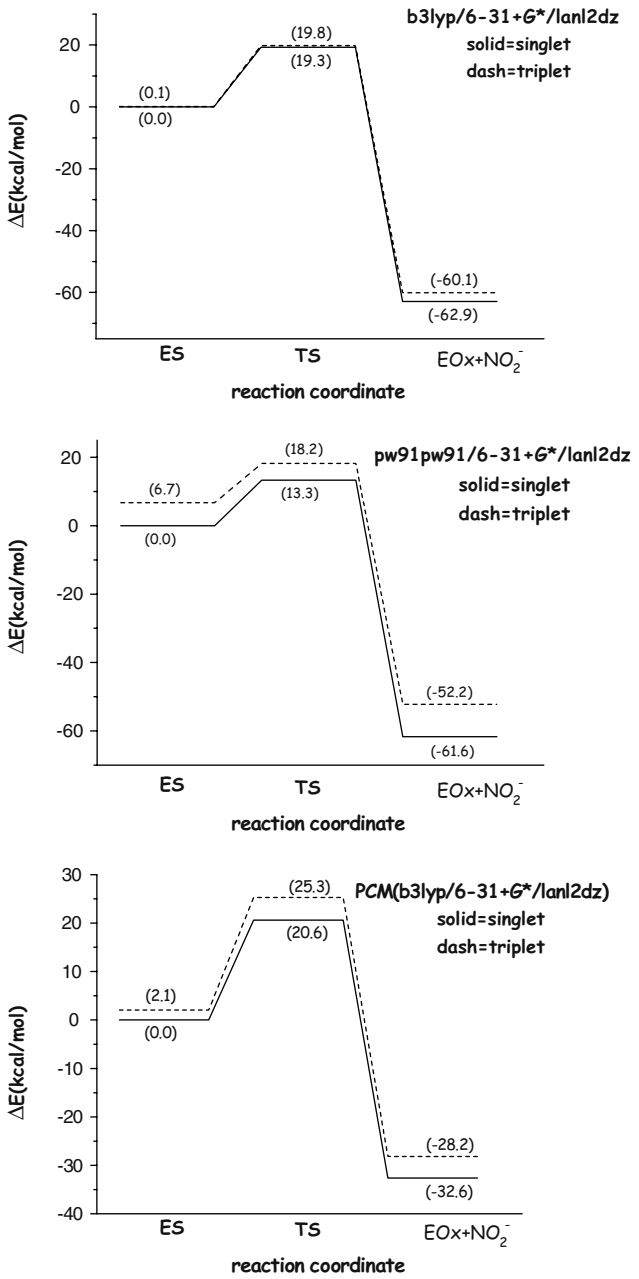

Fig. 4 Potential energy profiles for model A

The analogous system in the triplet electronic state presents as distorted trigonal bipyramidal geometry in which dithiolene sulphurs occupy both equatorial and axial positions (equatorial Mo–S mean distance is 2.465 Å, axial Mo–S mean distance is 2.365 Å).

Low- and high-spin energetic gap was found to be only 4.7 kcal/mol at B3LYP level, being the singlet the ground state.

Energetic profiles for both spin states are reported in Fig. 4 and the geometry of stationary points in Fig. 5.

The reaction begins with the formation the enzyme–substrate intermediate (ES) in which the NO_3^- is linked to metallic center through one of its oxygen atoms (Mo–$O^{nitrate}$ distance is 2.270 and 2.262 Å in the singlet and triplet state, respectively). After this interaction, the O–N bond length in the substrate lengthens slightly in both cases. The coordination geometry around molybdenum is different depending on electronic state. In particular it is trigonal prismatic and nearly octahedral, for singlet and triplet, respectively.

The low–high spin splitting relative to this intermediate was computed to be 0.1 kcal/mol, being also here the low spin the ground state.

In the transition state (TS) the Mo–$O^{nitrate}$ and $O^{nitrate}$–$N^{nitrate}$ distances assume the values of 1.913 (1.887) and 1.652 (1.685) Å, for singlet (triplet) spin states, respectively. The geometry in the low- and high-spin TSs appears to be very distorted with respect to the ideal trigonal prismatic and octahedral geometries of the starting ES complexes. The imaginary frequencies (589 cm^{-1} for singlet and 722 cm^{-1} for triplet) correspond to the stretching vibration mode of the Mo–$O^{nitrate}$ and $O^{nitrate}$–$N^{nitrate}$ bonds. The singlet and triplet TSs lie at 19.3 and 19.8 kcal/mol with respect to the ground-state ES complex, respectively.

The final products (EOxs in Fig. 5) possess a distorted geometry and lie at 62.9 kcal/mol (singlet) and at 60.1 kcal/mol (triplet) below the reference point. Mo–O bond has a length of 1.720 and 1.714 Å, for ground and excited states, respectively.

Our results are in qualitative agreement with the ones of Hall [118] and Thapper [120] for DMSO reductase, and with the experimental data on analogous molybdenum enzymes [119].

The transfer of the oxygen atom from the bound substrate to the metal center represents the rate-limiting step.

Computations were redone at PW91PW91 level in order to explore the possible dependence of singlet–triplet gap on the employed method or exchange-correlation functional.

The potential energy profiles obtained at PW91PW91, on B3LYP optimized geometries, were reported in Fig. 4.

As can be noted, despite both functionals indicate the singlet state as the ground one and predict similar exothermicity in the minimum energetic path, PW91PW91 enhances the gap between the spin states. The energetic barrier becomes lower especially in the case of singlet PES as can be expected from the fact that PWnPW91 functionals and B3LYP describe differently the long-range interactions [121–123].

Solvation energies computed at B3LYP level in the framework of self-consistent reaction field polarized

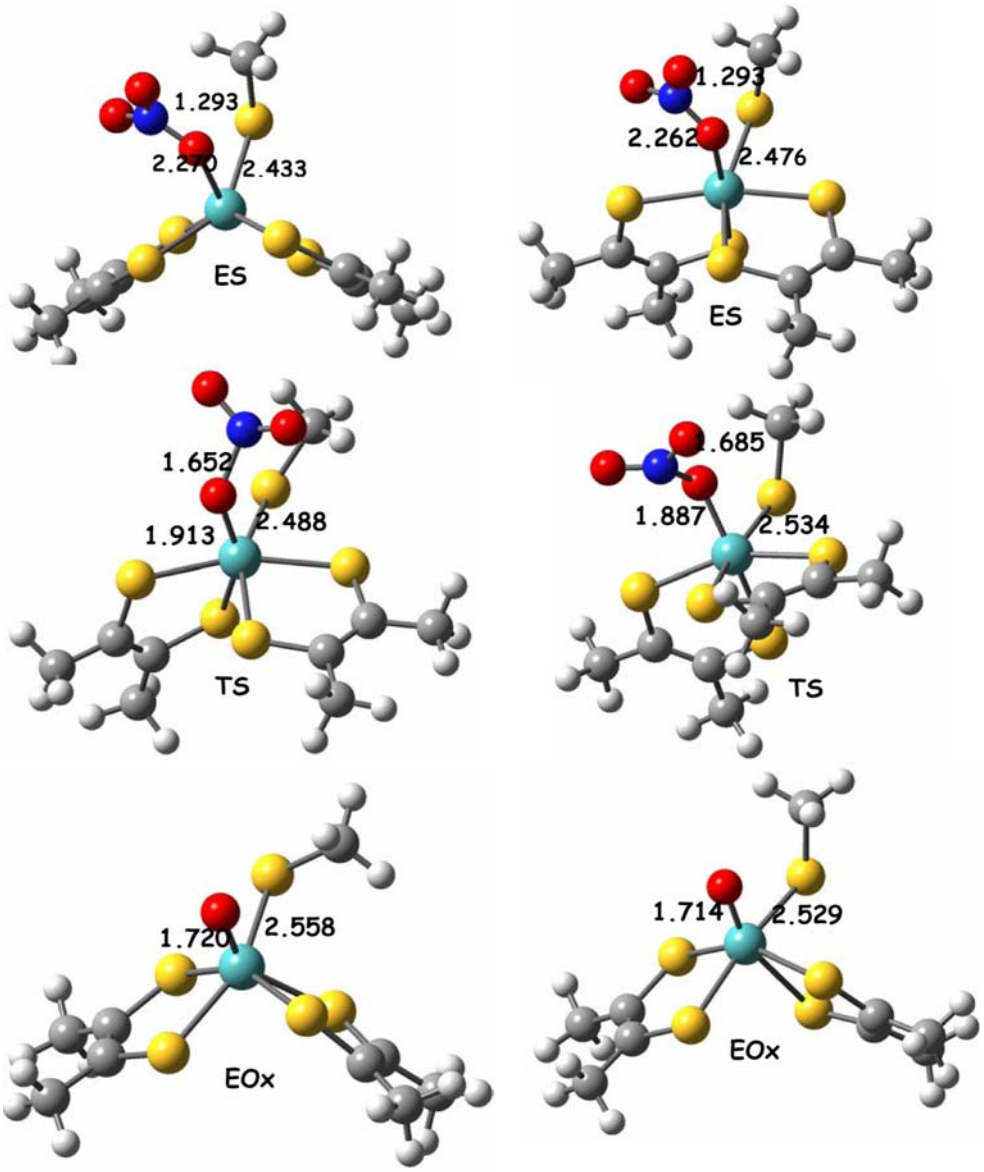

Fig. 5 Optimized geometries of ES, TS, and EOx species on singlet (on the *left*) and triplet (on the *right*) energy profiles

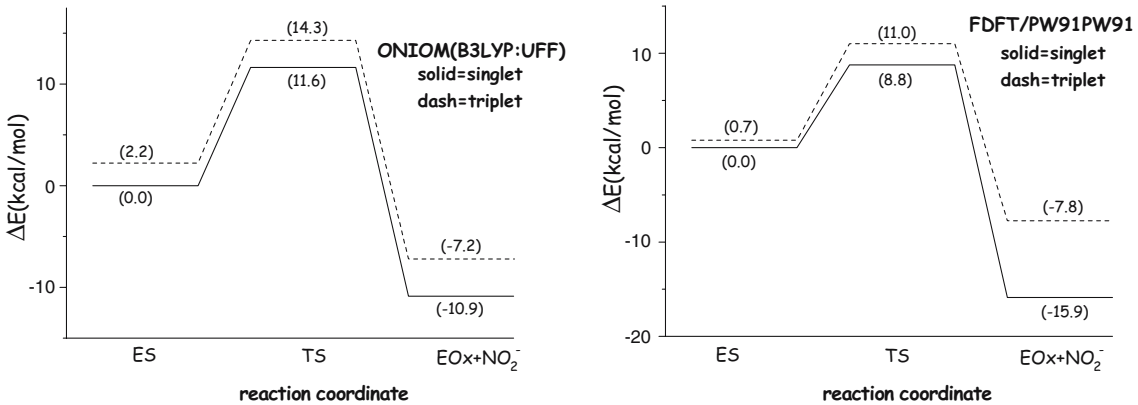

Fig. 6 Potential energy profile for model B

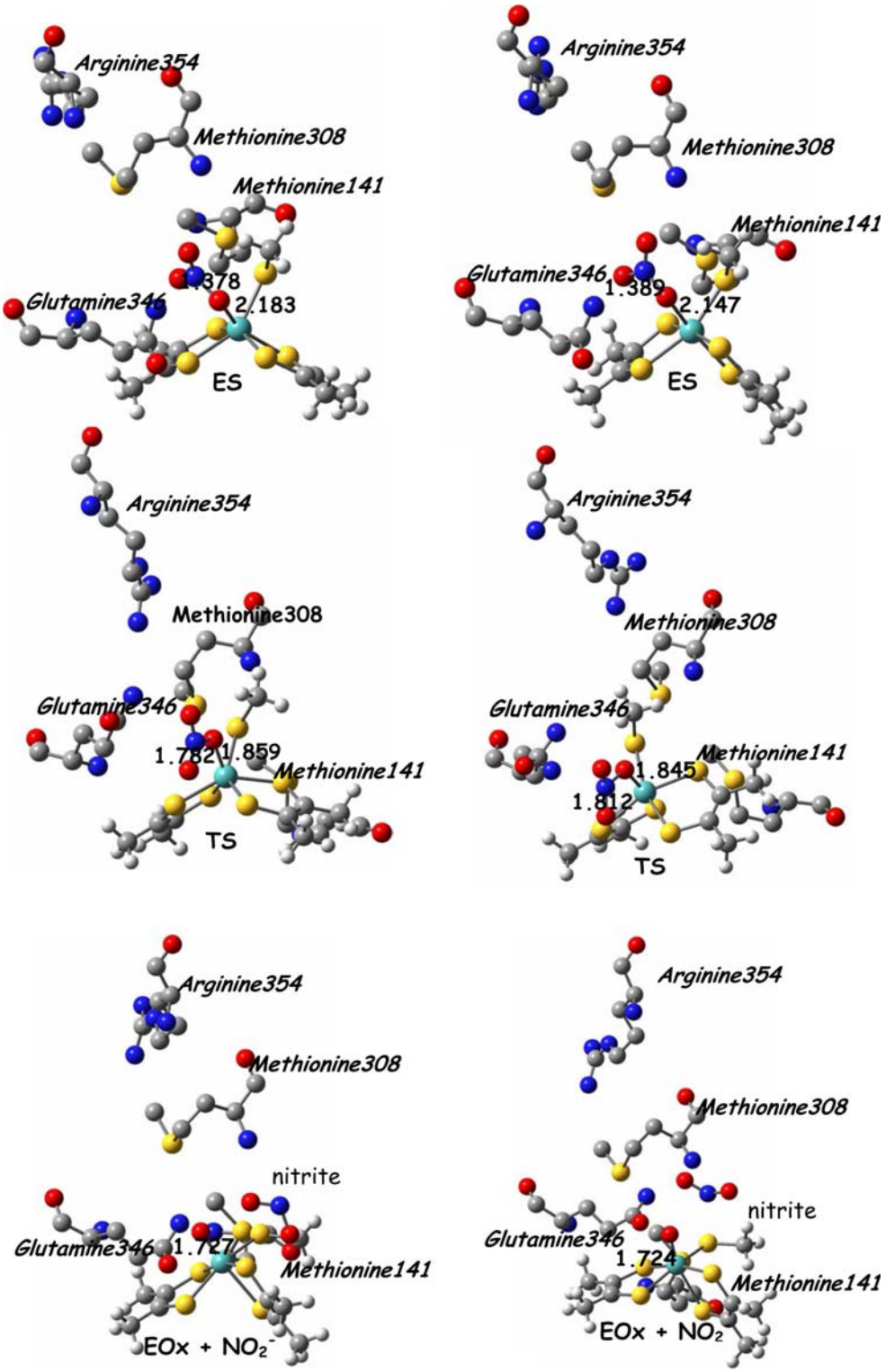

Fig. 7 Optimized geometries of ES, TS, and Eox + NO_2^- on singlet (on the *left*) and triplet (on the *right*) energy profiles

continuum model (SCRF-PCM) [47–49] using a dielectric constant value $\varepsilon = 4$ for describing the protein environment [45,46] indicate that, from a thermodynamic point of view, the reaction is less favored in solvent with respect to the gas phase (see Fig. 4). Furthermore, the triplet is to some extent destabilized with respect to the singlet state by protein environment and a slight increase of the low- and high-spin gap occurs at ES point.

On model B, ONIOM and orbital-free embedding computations, were performed.

ONIOM procedure was applied to the system described model B was divided into an inner layer consisting of the Mo^{IV} thiomethyl bisdithiolene complex, nitrate substrate and nitrite product molecules and an outer layer made up of Arg354, Met 141, Met308, and Gln346 amino acids at their crystallographic positions [58].

ONIOM energetic profiles for the enzyme in the singlet and triplet electronic states were reported in Fig. 6, while equilibrium structures on the PESs were depicted in Fig. 7.

In the ES complex, the Mo–$O^{nitrate}$ and $O^{nitrate}$–$N^{nitrate}$ distance values (2.183 and 1.378 Å for singlet and 2.147 and 1.389 Å for triplet) suggest that the interaction between the metal and the substrate oxygen atom is stronger than that found in the analogous complex with model A. The trigonal prismatic and octahedral arrangements around molybdenum in the low- and high-spin complexes appear to be much more distorted than in model A.

The ONIOM gap between the ES complexes in the singlet ground-state and in the excited triplet is 2.2 kcal/mol. This value compared to data obtained for model A indicate a certain dependence of the gap on the presence of protein environment.

No interaction was found between the metal bound nitrate molecule and the Arg354 residue. This result is not necessarily in disagreement with experimental data, since the supposed anchorage of substrate by means of the positive charge of Arg354 [117] could occur in a preliminary phase of the catalytic cycle.

The transition states for the singlet and triplet species are characterized by Mo–$O^{nitrate}$ and $O^{nitrate}$–$N^{nitrate}$ distances that are shorter and longer with respect to those of ES complexes, respectively.

Imaginary frequency values of 252 (singlet) and 444 (triplet) cm^{-1} can be attributed to the Mo–$O^{nitrate}$ and $O^{nitrate}$–$N^{nitrate}$ bonds stretching vibrational mode.

Transition states lie at 11.6 (singlet) and 14.3 (triplet) kcal/mol above the ES reference. The presence of the amino acid residues reduces, as can be noted, the barrier heights.

At 10.9 and 7.2 kcal/mol below the ES complex, for low- and high-spin case, respectively, we found the final products (EOx).

The low- and high-spin complexes EOx exhibit a similar octahedral geometry around molybdenum. The Mo–$O^{nitrate}$ distance is 1.727 and 1.724 Å, for singlet and triplet, respectively.

In the ONIOM treatment, the energy value of the product corresponds to a summation of the energy value of infinitely separated species ($E(\mathrm{EOx}) + E(\mathrm{NO_2^-})$). Since in the computations with model A it was impossible to obtain geometry convergence in the presence of a long-range interaction between nitrite and oxo-Mo^{VI} complex, the energetics obtained with the two different models cannot be compared as far as products are concerned.

ONIOM computations demonstrate that the protein environment has no influence on the mechanism followed by the enzymatic reaction but affects the kinetics lowering the activation barriers. In agreement with Morokuma [58] entatic principle, this can be explained considering the strain to which the active site is subjected in the presence of the protein environment. In fact, this strain acts as a device to accumulate energy which can be used to overcome barriers.

The equilibrium geometries obtained at the ONIOM (B3LYP:UFF) level were used to perform an orbital-free embedding analysis on model B. Single-point evaluation was obtained using GGA/PW91 [73] exchange-correlation functional.

Because of the differences between the used methodology, functional and basis set, no comparison is possible with ONIOM data; thus only the qualitative aspects of these last results will be discussed.

The potential energy profiles obtained applying the orbital-free embedding procedure for both singlet and triplet states are depicted in Fig. 6.

As in the previous cases, reaction proceeds most favorably along the singlet path.

Only 0.7 kcal/mol separate the low-spin ES complex from the same species having the triplet multiplicity.

The transfer of oxygen requires an activation energy of 8.8 kcal/mol for the low-spin and 11.0 kcal/mol for the high-spin. Products lie at 7.8 kcal/mol (singlet) and 15.9 kcal/mol (triplet) below the singlet ES complex.

Despite, the differences between ONIOM and orbital-free embedding methods, results appear to be very similar. However, it is worth underlining that the data obtained by the second treatment are characterized by the reliability peculiar to a totally quantum mechanical computation.

4 Conclusions

The potential-energy profiles for three prototype reactions catalyzed by bare and supported transition metals and by a metalloenzyme were reported in this paper. For these processes we have applied a number of quantum chemical methodologies developed for the treatment of complex reaction paths that define the state-of-the-art in this field. From the analysis of obtained data and on the basis of our experience, we can assert that available

theoretical tools are able, if properly used, to give reliable results allowing interpretation of incomplete experimental information. The examined cases suggest the following main conclusions:

- The use of simple models as those in gas-phase, provide structural and electronic information that can serve as guidelines for the study of more complex systems that are closer to the real life catalysts.
- In the description of catalytic processes particular attention must be devoted to the choice of the model to simulate the active site. For instance, in representing the enzyme active site, the addition of second shell residues is often crucial to define properly the reaction path. The most significant differences between the three descriptions examined here, seem to do not depend on the computational tool but on the choice of the model used to simulate the active site of the enzyme. In particular, the height of the activation barrier is quite affected by the presence of nearby amino acid residues that, inducing a certain strain in the catalytic core, enhances its reactivity.

Acknowledgments Financial support from the Università degli Studi della Calabria and Regione Calabria (POR Calabria 2000/2006, misura 3.16, progetto PROSICA) is gratefully acknowledged.

References

1. Schröder D, Schwarz H (1995) Angew Chem Int Ed 34:1973
2. Schwarz H, Schröder D (2000) Pure Appl Chem 72:2319
3. Plattner DA (2001) Int J Mass Spectrum 207:125
4. Ervin KM (2001) Int Rev Phys Chem 20:127
5. Zemski KA, Jurtes DR, Castleman AW Jr (2002) J Phys Chem B 106:6136
6. O_Hair RAJ, Khairallah GN (2004) J Cluster Sci 15:331
7. Chen P (2003) Angew Chem Int Ed 42:2832
8. Futrell JH (ed) (1986) Gaseous ion chemistry and mass spectrometry. Wiley, New York
9. Eller K, Schwarz H (1991) Chem Rev 91:1121
10. Modern mass spectrometry. (2003) In: Topics in current chemistry, vol 225. Springer, Berlin Heidelberg New York
11. Gross JH (2004) Mass spectrometry. Springer, Berlin Heidelberg New York
12. Thomas JM, Schlögl R (1994) Angew Chem Int Ed Engl 33:308
13. Cornils B, Herrmann WA (eds) (1996) Applied homogeneous catalysis with organometallic compounds, vol 1. VCH, Weinheim, pp 2
14. Thomas JM (1997) Chem Eur J 3:1557
15. Ertl G, Freund HJ (1999) Phys Today 52:32
16. Somorjai GA, McKrea K (2001) Appl Catal A 222:3
17. Notori R, Ohkuma T (2001) Angew Chem Int Ed 40:41
18. Ertl G (2002) J Mol Catal A 182/183:5
19. Bell AT (2003) Science 299:1688
20. Schlögl R, Hamid SBA (2004) Angew Chem Int Ed 43:1628
21. Zhang X, Chen X, Chen P (2004) Organometallics 23:3437
22. Stahl SS (2004) Angew Chem Int Ed 43:3400
23. Ajamian A, Gleason JL (2004) Angew Chem Int Ed 43:3754
24. Boudart M (2000) Catal Lett 65:1
25. Ertl G (2002) J Mol Catal A 182/183:5
26. Thomas JM, Catlow CRA, Sankar G (2002) Chem Commun 2921
27. de Bruin B, Budzelaar PHM, Wal AG (2004) Angew Chem Int Ed 43:4142
28. Copèret C, Chabanas M, Saint-Arromant RP, Basset J-M (2003) Angew Chem Int Ed 42:156
29. Hahn C (2004) Chem Eur J 10:5888
30. Reuter K, Frenkel D, Scheffler M (2004) Phys Rev Lett 93
31. Coates GW, Moore DR (2004) Angew Chem Int Ed 43:6618
32. van Santen RA, Neurock M (1995) Catal Rev Sci Eng 37:557
33. van Santen RA, Neurock M (2001) Encyclopedia of catalysis. Wiley, New York
34. van Santen RA (1997) J Mol Catal A Chem 115:405
35. Whitten JL, Yang H, (1996) Surf Sci Rep 24:59
36. Sauer J, Ugliengo P, Garrone E, Saunders VR (1994) Chem Rev 94:2095
37. Sauer J (1989) Chem Rev 89:199
38. Sauer J (1994) Zeolites and related microporous materials. In: State of the art 1994, vol 84
39. Sierka M, Sauer JJ (2000) Chem Phys 112:6983
40. Stampfl C, Ganduglia-Pirovano MV, Reuter K, Scheffler M (2001) Surf Sci 500
41. Hafner J (2000) Acta Mat 48:71
42. Hammer B, Nørskov JK (2000) Adv Catal 45:71
43. Hammer B, Nørskov JK (1997) In: Lambert RM, Pacchioni G (eds) Chemisorption and reactivity on supported clusters and thin films. Kluwer Academic, The Netherlands
44. Payne MC, Teter MP, Allan DC, Arias TA, Joannopoulos JD (1992) Rev Mod Phys 64:1045
45. Siegbahn PEM, Blomberg MRA (2000) Chem Rev 100:421
46. Noodleman L, Lovell T, Han W G, Li J, Himo F (2004) Chem Rev 104:459
47. Miertus S, Tomasi J (1982) Chem Phys 65:239
48. Cossi M, Barone V, Commi R, Tomasi J (1996) Chem Phys Lett 255:327
49. Barone V, Cossi M, Menucci B, Tomasi J (1997) J Chem Phys 107:3210
50. Warshel A (1991) Computer modeling of chemical reactions in enzymes and solutions. Wiley, New York
51. Maseras F, Morokuma K (1995) J Comp Chem 16:1170
52. Humbel S, Sieber S, Morokuma K (1996) J Chem Phys 105:1959
53. Matsubara T, Sieber S, Morokuma K (1996) Int J Quant Chem 60:1101
54. Svensson M, Humbel S, Froese RDJ, Matsubara T, Sieber S, Morokuma K (1996) J Phys Chem 100:19357
55. Svensson M, Humbel S, Morokuma K (1996) J Chem Phys 105:3654
56. Dapprich S, Komáromi I, Byun KS, Morokuma K, Frisch MJ (1999) J Mol Struct (Theochem) 462:1
57. Vreven T, Morokuma K (2000) J Comp Chem 21:1419
58. Torrent M, Vreven T, Musaev DG, Morokuma K, Farkas O, Schlegel HB (2002) J Am Chem Soc 124:192
59. Rappé AK, Casewit CJ, Colwell KS, Goddard III WA, Skiff WM (1992) J Am Chem Soc 114:10024
60. Wesolowski TA, Warshel A (1993) J Phys Chem 97:8050
61. Hong G, Strajbl M, Wesolowski TA, Warshel A (2000) J Comp Chem 21:1554
62. Frisch MJ, Trucks GW, Schlegel HB, Scuseria GE, Robb MA, Cheeseman JR, Montgomery JA, Jr, Vreven T, Kudin KN,

Burant JC, Millam JM, Iyengar SS, Tomasi J, Barone V, Mennucci B, Cossi M, Scalmani G, Rega N, Petersson GA, Nakatsuji H, Hada M, Ehara M, Toyota K, Fukuda R, Hasegawa J, Ishida M, Nakajima T, Honda Y, Kitao O, Nakai H, Klene M, Li X, Knox JE, Hratchian HP, Cross JB, Bakken V, Adamo C, Jaramillo J, Gomperts R, Stratmann RE, Yazyev O, Austin AJ, Cammi R, Pomelli C, Ochterski JW, Ayala PY, Morokuma K, Voth GA, Salvador P, Dannenberg JJ, Zakrzewski VG, Dapprich S, Daniels AD, Strain MC, Farkas O, Malick DK, Rabuck AD, Raghavachari K, Foresman JB, Ortiz JV, Cui Q, Baboul AG, Clifford S, Cioslowski J, Stefanov BB, Liu G, Liashenko A, Piskorz P, Komaromi I, Martin RL, Fox DJ, Keith T, Al-Laham MA, Peng CY, Nanayakkara A, Challacombe M, Gill PMW, Johnson B, Chen W, Wong MW, Gonzalez C, Pople JA (2004) Gaussian Inc., Wallingford CT
63. Dulak M, Wesolowski TA (2005) Int J Quantum Chem 10:543
64. Köster AM, Flores-Moreno R, Geudtner G, Goursot A, Heine T, Reveles JU, Vela A, Salahub DR, *deMon*: Program:version:1_2.2003, NRC, Canada
65. Becke AD (1993) J Chem Phys 98:5648
66. Lee C, Yang W, Parr RG (1988) Phys Rev B 37:785
67. Hay PJ, Wadt WR (1985) J Chem Phys 82:270
68. Hay PJ, Wadt WR (1985) J Chem Phys 82:284
69. Hay PJ, Wadt WR (1985) J Chem Phys 82:299
70. Krishnan R, Binkley JS, Seeger R, Pople JA (1980) J Chem Phys 72:650
71. Blaudeau JP, McGrath MP, Curtis LA, Radom L (1997) J Chem Phys 107:5016
72. Burke K, Perdew JP, Wang Y (1998) In: Dobson JF, Vignale G, Das MP (eds) Electronic density functional theory: recent progress and new directions. Plenum, New York
73. Perdew JP (1991) In: Ziesche P, Eschrig H (eds) Electronic structure of solids '91, vol 11
74. Perdew JP, Chevary JA, Vosko SH, Jackson KA, Pederson MR, Singh DJ, Fiolhais C (1992) Phys Rev B 46
75. Perdew JP, Chevary JA, Vosko SH, Jackson KA, Pederson MR, Singh DJ, Fiolhais C (1993) Phys Rev B 48
76. Perdew JP, Burke K, Wang Y (1996) Phys Rev B 54:16533
77. Godbout N, Salahub DR, Andzelm J, Wimmer E (1992) Can J Chem 70:560
78. The deMon User's Guide, Version 1.0.3, 2003–2004
79. Benson SW (1968) Thermochemical kinetics. Wiley, New York
80. Houk KN, Gandour RW, Strozier RW, Rondan NG, Paquette LA (1979) J Am Chem Soc 101:6797
81. Bach RD, Wolber GJ, Schlegel HB (1985) J Am Chem Soc 107:2837
82. Tysoe WT, Nyberg GL, Lambert RM (1983) J Chem Soc Chem Commun 623
83. Sesselmann WS, Woratschek B, Ertl G, Kuppers J, Haberland H (1983) Surf Sci 130:245
84. Gentle TM, Muetterties EL (1983) J Phys Chem 87:2469
85. Holmblad PM, Rainer DR, Goodman DW (1997) J Phys Chem B 101:8883
86. Abdelrehim IM, Pelhos K, Madey TE, Eng J, Chen JG (1998) J Mol Catal A 131:107
87. Rucker TG, Logan MA, Gentle TM, Muetterties EL, Somorjai GA (1986) J Phys Chem 90:2703
88. Patterson CH, Lambert RM (1988) J Am Chem Soc 110:6871
89. Zhu XY, White JM (1989) Surf Sci 214:240
90. Mate CM, Kao CT, Bent BE, Somorjai GA (1988) Surf Sci 197:183
91. Ormerod RM, Lambert RM (1992) J Phys Chem 96:8111
92. Ormerod RM, Lambert RM, Hoffmann H, Zaera F, Yao JM, Saldin DK, Wang LP, Bennet DW, Tysoe WT (1993) Surf Sci 295:277
93. Pacchioni G, Lambert RM (1994) Surf Sci 304:208
94. Hoffmann H, Zaera F, Ormerod RM, Lambert RM, Yao JM, Saldin DK, Wang LP, Bennett DW, Tysoe WT (1992) Surf Sci 268:1
95. Abbet S, Sanchez A, Heiz U, Schneider WD, Ferrari AM, Pacchioni G, Rösch N (2000) J Am Chem Soc 122:3453
96. Abbet S, Sanchez A, Heiz U, Schneider WD (2001) J Catal 198:122
97. Ferrari AM, Giordano L, Pacchioni G, Abbet S, Heiz U (2002) J Phys Chem B 106:3173
98. Judai K, Wörz AS, Abbet S, Antonietti JM, Heiz U, Del Vitto A, Giordano L, Pacchioni G (2005) Phys Chem Chem Phys 7:955
99. Chrétien S, Salahub DR (2003) J Chem Phys 119:12291
100. Buckner SW, MacMahon TJ, Byrd GD, Freiser BS (1989) Inorg Chem 28:3511
101. Schröder D, Shaik S, Schwarz H (2000) Acc Chem Res 33:139
102. Armentrout PB, Beauchamp JL (1989) Acc Chem Res 22:315
103. Armentrout PB (1991) Science 251:175
104. Moore CE (1991) Atomic energy levels, vol 1. NSRD-NBS, USA. U.S. Government Printing Office, Washington DC
105. Dewar MJS (1951) Bull Soc Chim Fr 79
106. Chatt J, Duncanson LA (1953) J Chem Soc 2939
107. Frenking G, Fröhlich N (2000) Chem Rev 101:717
108. Ferrari AM, Giordano L, Rösch N, Heiz U, Abbet S, Sanchez A, Pacchioni G (2000) J Phys Chem 104:10612
109. Hardesty JH, Koerner JB, Albright AT, Lee GY (1999) J Chem Soc 121:6055
110. Ormerod RM, Baddeley J, Lambert RM (1991) Surf Sci Lett 259:L709
111. Kaltchev M, Stacchiola D, Molero H, Wu G, Blumenfeld A, Tysoe WT (1999) Catal Lett 60:11
112. Ferrari AM, Giordano L, Pacchioni G, Abbet S, Heiz U (2002) J Phys Chem B 106:3173
113. Pacchioni G, Bagus PS, Parmigiani F (eds) (1992) Cluster models for surface and bulk phenomena, NATO ASI Series B, vol 283. Plenum, New York
114. Nygren MA, Pettersson LGM, Barandiaran Z, Seijo L (1994) J Chem Phys 100:2010
115. Ferrari AM, Giordano L, Pacchioni G, Abbet S, Heiz U (2002) J Phys Chem B 106:3173
116. Craig A, Holm RH (1989) J Am Chem Soc 111:2111
117. Dias MJ, Than ME, Humm A, Huber R, Bourenkov GP, Bartunik HD, Bursakov S, Calvete J, Caldeira J, Carneiro C, Moura JJG, Moura I, Romao MJ (1999) Structure 7:65
118. Webster CE, Hall MB (2001) J Am Chem Soc 123:5820
119. Wang JJ, Kryatova OP, Rybak-Akimova EV, Holm RH (2004) Inorg Chem 43:8092
120. Thapper A, Deeth RJ, Nordlander E (2002) Inorg Chem 41:6695
121. Porembski M, Weisshaar JC (2001) J Phys Chem A 105:4851
122. Jursic BS (1998) J Mol Struc 430:17
123. Nachtigall P, Jordan KD, Smith A, Jonsson H (1996) J Chem Phys 104:148